Optics Letters

Gold-induced photothermal background in on-chip surface enhanced stimulated Raman spectroscopy

Kristof Reynkens,[1,2,*] Stéphane Clemmen,[1,2,3,4] Haolan Zhao,[1,2] Ali Raza,[1,2,5] Tom Vanackere,[1,2] Andim Stassen,[6] Michiel Van Daele,[7] Jolien Dendooven,[7] and Roel Baets[1,2]

[1]Photonics Research Group, Department of Information Technology, Ghent University-IMEC, Technologiepark 126, 9052 Ghent, Belgium
[2]Center for Nano- and Biophotonics, Ghent University, 9052 Ghent, Belgium
[3]Laboratoire d'Information Quantique, Université Libre de Bruxelles, 1050 Brussels, Belgium
[4]OPERA-Photonique CP 194/5, Université Libre de Bruxelles (ULB), 1050 Brussels, Belgium
[5]Currently with Microsoft, Keilalahdentie 2-4, 02150 Espoo, Finland
[6]Imec, Kapeldreef 75, B-3001 Leuven, Belgium
[7]Department of Solid State Sciences, CoCooN Research Group, Krijgslaan 281/51, Ghent 9000, Belgium
*Corresponding author: Kristof.Reynkens@UGent.be

Received 28 December 2020; revised 14 January 2021; accepted 14 January 2021; posted 14 January 2021 (Doc. ID 418527); published 16 February 2021

Surface enhanced Raman spectroscopy (SERS) and stimulated Raman spectroscopy (SRS) are well established techniques capable of boosting the strength of Raman scattering. The combination of both techniques (surface enhanced stimulated Raman spectroscopy, or SE-SRS) has been reported using plasmonic nanoparticles. In parallel, waveguide enhanced Raman spectroscopy has been developed using nanophotonic and nanoplasmonic waveguides. Here, we explore SE-SRS in nanoplasmonic waveguides. We demonstrate that a combined photothermal and thermo-optic effect in the gold material induces a strong background signal that limits the detection limit for the analyte. The experimental results are in line with theoretical estimates. We propose several methods to reduce or counteract this background. © 2021 Optical Society of America

https://doi.org/10.1364/OL.418527

Raman spectroscopy has proven to be a useful sensing technique due to its capability of identifying a diverse set of analytes based on their molecular vibrational fingerprints. However, Raman scattering is inherently a weak process, so Raman spectroscopy systems are complex and costly (i.e., a high power laser, a spectrometer with a deeply cooled charge-coupled device (CCD) camera and a confocal Raman microscope). Arguably, the most critical part of a Raman system is the detector as it needs to cope with extremely low light levels and has to present enough pixels to resolve a spectrum spanning over several thousands of wavenumbers. Given the exceptional technological maturity of the CCD camera, a large effort has recently been focused on increasing the amount of light that can be captured by the detector. In that context, stimulated Raman spectroscopy (SRS) has emerged as a way to accelerate the acquisition of Raman spectra [1,2].

Miniaturized and low cost alternatives for performing Raman spectroscopy have recently been investigated by bringing various parts of a Raman system on a photonic chip: spectrometer [3], notch filter [4], and lasers [5].

In this context of integration of a Raman system, there have been several successful attempts to increase the Raman signal by using nanophotonic structures such as dielectric [6,7] and plasmonic structures [8,9]. Nanoplasmonic waveguides [8] turned out to be advantageous over dielectric waveguides since they do not suffer from the significant photoemission background that is characteristic of dielectric materials [10]. Moreover, those metallic slot waveguides exhibit a plasmonic enhancement that is nonresonant and well controlled by e-beam-free nanofabrication. While the scattering enhancement provided by these plasmonic waveguides is nearly on par with the best surface enhanced Raman spectroscopy (SERS) substrates, this is still not enough to avoid the use of an expensive deeply cooled camera. Stimulation with a Stokes beam can boost the Raman signal by many orders of magnitude. This has been demonstrated on plasmonic nanoparticles using surface enhanced stimulated Raman spectroscopy (SE-SRS) together with ultrafast pulses [11–13] (and more recently CW beams [14]) and by on-chip SRS measurements using CW beams and dielectric waveguides [15]. In comparison to that latter demonstration, the use of a nanoplasmonic waveguide instead of a dielectric one promises major advantages. Indeed, it was previously shown that the combination of plasmonic enhancement and a rather long interaction length (in comparison to the interaction length in common SERS substrate) leads to a large Raman scattering enhancement [8] so that the required pump and Stokes fields can be of very low power and therefore integration on a photonic integrated circuit (PIC) becomes easier. Moreover, we know that dielectric waveguides suffer from a broadband photoemission

that superposes itself onto the Raman spectrum while gold plasmonic waveguides suffer far less from it [8,10,16,17].

In this Letter, we first make a theoretical comparison between waveguide-based SRS and SE-SRS relying on a nanoplasmonic waveguide as in [8]. Then, we present our experiment and results. Those results reveal a response much stronger than expected that cannot be explained by a Raman scattering process. Further investigations are performed that confirm a combined photothermal and thermo-optic effect in gold. This effect was already suggested in [12,18], but here we demonstrate for the first time that the experimental results confirm theoretical estimates for the effect. We conclude by proposing a few routes to perform successful SE-SERS using nanoplasmonic waveguides.

For comparing SRS in different waveguides, let us set the typical dimensions of a Si_3N_4 dielectric strip waveguide as in [15] : width × thickness × length = 700 nm × 300 nm × 8 mm. The geometry of the nanoplasmonic waveguide [8] is a short gold slot waveguide 1.8 μm long, with a gap of 15 nm (depending on the sample) for a gold thickness in the gap of 5.5 nm and a total width of 0.88 μm (see Fig. S1 and Section 1 of Supplement 1 for an illustration and greater detail about the geometry and the fabrication). Assuming the same analyte [a monolayer of 4-Nitrothiophenol (NTP)] as well as a guided pump and Stokes power of 1 mW and 4 mW, respectively (with 1 mW being the modulated pump power), the 1.8-μm-long nanoplasmonic slot waveguide is expected to generate a Stokes power 70.4 times greater than the one generated in a 8-mm-long dielectric strip waveguide. More importantly, the plasmonic waveguide experiences a photoemission background 2.3×10^{-4} lower than the corresponding dielectric waveguide. Supporting calculations are provided in Section 2 of Supplement 1.

The SE-SRS experiment is performed with the setup presented in Fig. 1 and validated in a previous study [15]. The pump and Stokes beams are counterpropagating in order to ease the separation of both beams prior to detection. The pump beam is originating from a laser diode and is sinusoidally modulated via its current resulting in a modulation depth with an amplitude of 30% (peak-to-peak) at the wavelength of 785 nm. The Stokes beam is originating from a tunable CW Ti:sapphire laser. The Stokes beam is eventually measured using a balanced detector to remove any fluctuation from the source itself (built-in gain of 10^5). The Raman gain in the sample imprints a shallow modulation on the Stokes beam that is picked up by a lock-in amplifier. Special care is taken to avoid the creation of cavities within the setup: the facets of the waveguide are polished at an angle so that Fresnel reflection does not couple back to the waveguides, and the entire chip is set at an angle so that any stray light being guided in the optical cladding cannot find its way to the other side of the chip. The proper operation of our setup is confirmed by the acquisition of a SRS spectrum obtained with a dielectric waveguide and showing perfect agreement with the corresponding spontaneous Raman spectrum (see Fig. S2 in Supplement 1).

The plasmonic waveguide samples are functionalized with a monolayer of NTP used as the model molecule for Raman sensing in this work. This molecule is chosen because it binds selectively to gold but not to silicon nitride avoiding any extra contribution of SRS from the access waveguides themselves. We have two types of samples that differ by the way the gold deposition is performed: sputtering [8] or atomic layer deposition

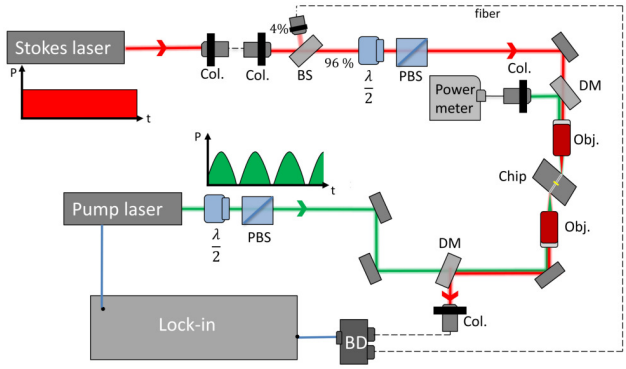

Fig. 1. Schematic of the setup for the SE-SRS measurements. λ/2, half-wave plate; PBS, polarization beam splitter aligned to the TE-polarizion of the waveguide; DM, dichroic mirrors; Col., collimators; Obj., Mitutoyo Plan Apo 50× (NA = 0.65); BD, balanced detector; BS, 4%-reflective beam splitter.

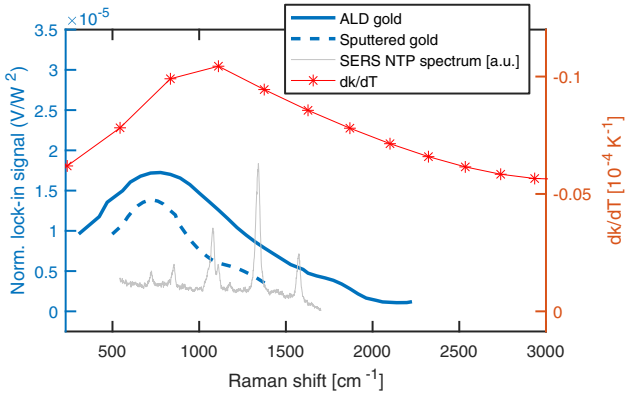

Fig. 2. Recorded spurious SRS spectra for the plasmonic slot made with ALD gold (bold blue curve and left axis) and sputtered gold (dotted blue curve and left axis). Wavelength dependence of the extinction coefficient dk/dT of gold (red curve and right axis) [20]. Indicative Raman spectra of NTP obtained using a regular spontaneous Raman setup and the sample under investigation are shown in gray in (arbitrary units).

(ALD) [19]. A detailed description of the sample preparation can be found in Section 1 of Supplement 1.

The results of the measurements are presented in Fig. 2, while the modulation frequency was set to 1 MHz, the lock-in amplifier to a 500 ms time constant, and the optical power 25 mW and 20 mW before the objectives for the pump and Stokes beams, respectively. The presented spectra are obtained by averaging two successive measurements, applying a Savitzky–Golay filter, and normalizing by the pump and Stokes power.

The presented spectra (in blue) are obviously not showing the NTP peaks we are expecting. The light gray curve shows the expected NTP spectrum and has been taken via spontaneous Raman measurements on the nanoplasmonic slot waveguides. The spectra also do not match the photoemission signature that we can observe from the dielectric waveguides that we can see in Fig. S2. Moreover, the response obtained in Fig. 2 far exceeds the one we can observe using a dielectric waveguide. The lock-in signal obtained for a dielectric slot waveguide is 2.5×10^{-5} V corresponding to a modulation depth $\Delta I_s / I_s = 4.7 \times 10^{-6}$. In comparison, the lock-in signal captured for the plasmonic

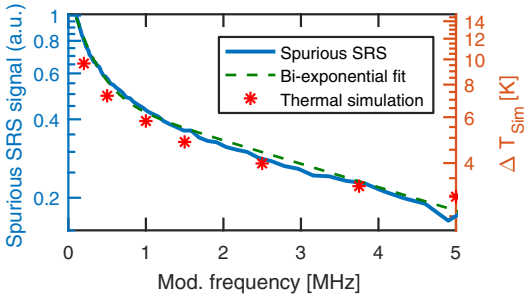

Fig. 3. Effect of the modulation frequency on the recorded spurious SRS signal (blue curve and left axis) and bi-exponential fit (dashed green). Amplitude of the thermal modulation ΔT_{sim} at the waveguide from time-dependent simulations (red stars and right axis).

waveguide is $1.5 - 2 \times 10^{-4}$ V corresponding to a modulation depth of $4.46 - 5.95 \times 10^{-4}$. This is much more than the modulation depth from the NTP monolayer expected to be 5.6×10^{-6}. The contribution of the dielectric access waveguides to this signal is completely negligible here because its is shorter and experiences more loss than the reference waveguide.

To explain the observed spectrum, we have to look elsewhere. It has been reported before that competing heterodyne optical processes such as photothermal effects, cross-phase modulation (XPM), two-photon absorption (TPA), and transient absorption (TA) can result in a large (thermal) background spectrally overlapping with the (SE-)SRS signal [12,21]. Among those effects, some are fast (ps or faster), while others may be slow enough to be dependent on the frequency of the modulation we impart on the pump beam [22]. We have, therefore, investigated this response using the lock-in as a function of the modulation frequency (fixing the Stokes wavelength to 834 nm). The result is presented in Fig. 3 and shows a clear decrease of the response for increasing modulation frequency. This points to a slow effect such as a thermal effect, with the others being considerably faster [23]. A closer look at the result presented in Fig. 3 reveals that the decay is best fitted by a bi-exponential. This may hint at the presence of two phenomena with different time scales.

The thermal effect that could account for our large response is a combined photothermal and thermo-optic effect explained as follows. A modulated heating of the gold occurs via absorption of the modulated pump beam. This periodic heating affects the absorption and refractive index of the gold [24] that in turn modulates the Stokes beam. The change of the refractive index and absorption with temperature are quantified via the thermo-refractive coefficient (dn/dT) and thermo-extinction coefficient (dk/dT). These coefficients vary with the wavelength, and we present the thermo-extinction coefficient measured by Wilson *et al.* [20] in Fig. 2 (red line). This spectrum is remarkably close to the spectra we have measured, hinting at an effect dominated by the thermo-optic absorption. One should note that the contribution of the thermo-refractive coefficient was dominant in a recent SE-SRS experiment [12,18] relying on a confocal microscope. In the present case, a contribution of the thermo-refractive effect to the signal collected in the lock-in amplifier is also possible. Indeed, the presence of a weak cavity in combination with a modulation of the refractive index would lead to a modulated Stokes signal. Such cavity can be formed by the mode mismatch at the transition between the nanoplasmonic waveguide and the dielectric slot serving as access waveguides. However, the presence of such a cavity should be evidenced by the fringe pattern characteristic of a Fabry–Perot cavity. Given the geometry of the nanoplasmonic waveguide, the group index for the plasmonic mode is $n_g = 6.8$ (from modeling using Lumerical mode solutions), which gives a free-spectral range $\text{FSR} = \lambda_s^2/(n_g L) = 58$ nm for a cavity length $L = 1.8$ μm at a wavelength $\lambda = 841$ nm. A transmission measurement carried over 150 nm shows no evidence of a cavity. Therefore, the thermo-optic absorption seems a better candidate to explain our spectra. Making a calculation of the strength of this thermal effect using a value of $dk/dT = -0.1045 \times 10^{-4}\ \text{K}^{-1}$ [20] shows that even a modest temperature modulation depth (peak-to-peak) $\Delta T_{\text{Exp}} = 2.5$ K is sufficient to induce our experimentally captured spurious modulation depth on the Stokes intensity. In the same way, a calculation can be made using $dn/dT = 2 \times 10^{-4}\ \text{K}^{-1}$ and an equivalent ΔT_{Exp}, which shows the maximum modulation depth due to the Fabry–Perot cavity is an order of magnitude smaller ($\Delta I_s / I_s = 1.4 \times 10^{-5}$), which agrees with our earlier statement. In order to investigate this further, we performed a time-dependent thermal simulation of our system using COMSOL multiphysics. We defined a custom-built 3D model of our device that includes the gold part of the nanoplasmonic waveguide, its silicon nitride core, the optical cladding, and the substrate. More details about the model and the simulation can be found in Section 4 of Supplement 1. The result of this time-dependent thermal simulation carried out for the experimental conditions associated with Fig. 2 shows that the temperature rises from 293.5 K to 349 K after 10 μs in quasi steady state with a remaining temperature modulation, the amplitude of which is $\Delta T_{\text{Sim}} = 5.8$ K. The estimated ΔT_{Exp} corresponds reasonably well with what can be expected from simulations. The small discrepancy could be due to uncertainties in the very details of the geometry of the plasmonic waveguide (the size of the slot gap) as well as the coupling loss between plasmonic and dielectric waveguides (as it relates to the amount of light actually absorbed by the gold nanostructure).

This thermal simulation can also be confronted to the result presented in Fig. 3. Remarkably, the simulation reproduces the bi-exponential behavior we deduced from our measurement. By simulating the amplitude of the thermal modulation at various positions in the vicinity of the plasmonic waveguide, we can understand why two time scales are characteristic of the heat flow out of the waveguide. Figures 4(a) and 4(b) illustrate the geometry of our structure in the transverse plane (cross section) and from the top, respectively. The "steady state" thermal modulation amplitudes ΔT_{sim} at the positions denoted by letters A–J in Figs. 4(a) and 4(b) are summarized in Fig. 4(c). This shows that the heat flows better along the X axis than it does over the Y and Z axes. This is actually meaningful since the gold layer making the plasmonic waveguide extends in a narrow strip extending 6 μm on each side along the X direction. The thermal resistivity of that gold strip is lower than the one of the silica cladding and silicon substrate associated to the heat flow along the Y axis, and it is also lower than the thermal resistivity of the silicon nitride associated to the heat flux along the Z axis. Hence, higher modulation frequencies are supported in the gold compared to the surrounding materials.

We believe all this evidence is clearly pointing at the thermo-optic absorption mechanism to explain our spectra in Fig. 2. A remaining question can be raised concerning the wavelength

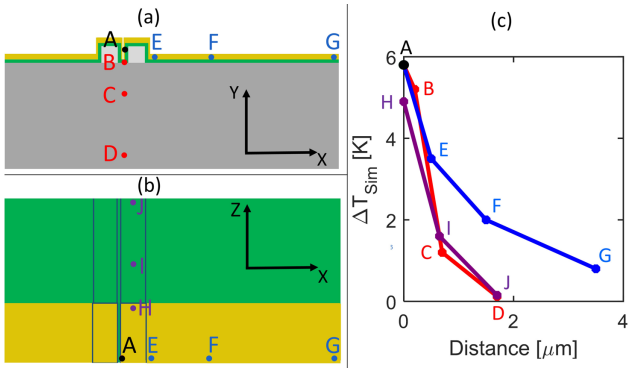

Fig. 4. (a) Cross section of the plasmonic slot with thermal monitors placed in the plasmonic slot (A,B), the silica (C, D), and along the gold sheet (E, F, G). (b) Top-down view of the slot. Monitors are placed along the propagating direction in the Si_3N_4 core (H, I, J). (c) Variation of the thermal modulation (ΔT_{Sim}) with distance.

shift of our spectra as compared with the one of the thermo-extinction coefficient. A possible explanation could be that the thermo-extinction coefficient does not scale perfectly linearly with temperature. As the reported curve originating from [20] was obtained at temperatures from 298.15 K to 430.15 K, this may have some impact. As we reported previously, the field enhancement associated with our plasmonic waveguide is mostly nonresonant and, thus, is spectrally far broader than the spectra depicted in Fig. 2. As compared to sputtered gold samples [8], the ALD gold ones present a slightly more resonant field enhancement due to the presence of nanostructured gaps within the material that allow localized plasmons resonances [19]. We cannot reliably infer any difference between ALD and the sputtered gold sample in the present investigation.

Both in the present case or in the free-space demonstration of SE-SRS reported in [18], the photothermal/thermo-optic effect can in principle be mitigated. One obvious mitigation strategy consists of increasing the modulation frequency as lock-in systems operating at hundreds of MHz exist. Ultrafast SRS techniques may also suffer less from the thermal effects [11]. Another mitigation procedure consists of removing the thermal modulation without affecting the Raman signal itself. This could be achieved by using a second pump beam in anti-phase with the first one so that the heating is constant at all time. The auxilliary pump beam could be set at a different wavelength either sufficiently remote from the first pump so as to avoid any Stokes response in the region of interest or close to the first pump, in which case two identical superimposed but shifted spectra will be measured and signal processing is needed to disentangle them.

In conclusion, we have shown that while SE-SRS using nanoplasmonic waveguides is appealing, it comes with challenges. The heating intrinsic to linear absorption in the gold nanostructure induces a thermo-optic effect that affects the Stokes beam overshadowing the Raman signature of the analyte (NTP in the present case). Not only is this thermo-optic effect 2 orders of magnitude stronger than the Raman response, but it also presents its own non-trivial spectrum. We have introduced mitigation strategies that may be combined in future investigations in order to realize the actual potential of nanoplasmonic-based SE-SRS.

Funding. Fonds De La Recherche Scientifique-FNRS; Vlaamse regering (Methusalem grant (R. Baets) "Smart Photonic Chips").

Acknowledgment. The authors acknowledge S. T. Barry and M. B. E. Griffiths for their contributions regarding the synthesis of the Au ALD precursor [19] and R. Wilson and D. G. Cahill for sharing unpublished data [20].

Disclosures. Stéphane Clemmen is a research associate of the Fonds De La Recherche Scientifique-FNRS.

Supplemental document. See Supplement 1 for supporting content.

REFERENCES

1. D. Fu, G. Holtom, C. Freudiger, X. Zhang, and X. S. Xie, J. Phys. Chem. B **117**, 4634 (2013).
2. C. L. Lee and K. Hewitt, Faraday Discuss. **205**, 227 (2017).
3. E. Ryckeboer, X. Nie, A. Z. Subramanian, D. Martens, P. Bienstman, S. Clemmen, S. Severi, R. Jansen, G. Roelkens, and R. Baets, Proc. SPIE **9891**, 98911K (2016).
4. X. Nie, N. Turk, Y. Li, Z. Liu, and R. Baets, Opt. Lett. **44**, 2310 (2019).
5. E. Haglund, M. Jahed, J. S. Gustavsson, A. Larsson, J. Goyvaerts, R. Baets, G. Roelkens, M. Rensing, and P. O'Brien, Opt. Express **27**, 18892 (2019).
6. A. Dhakal, A. Z. Subramanian, P. Wuytens, F. Peyskens, N. L. Thomas, and R. Baets, Opt. Lett. **39**, 4025 (2014).
7. S. A. Holmstrom, T. H. Stievater, D. A. Kozak, M. W. Pruessner, N. Tyndall, W. S. Rabinovich, R. A. McGill, and J. B. Khurgin, Optica **3**, 891 (2016).
8. A. Raza, S. Clemmen, P. Wuytens, M. Muneeb, M. Van Daele, J. Dendooven, C. Detavernier, A. Skirtach, and R. Baets, APL Photon. **3**, 116105 (2018).
9. Q. Cao, J. Feng, H. Lu, H. Zhang, F. Zhang, and H. Zeng, Opt. Express **26**, 24614 (2018).
10. N. L. Thomas, A. Dhakal, A. Raza, F. Peyskens, and R. Baets, Optica **5**, 328 (2018).
11. R. R. Frontiera, A.-I. Henry, N. L. Gruenke, and R. P. Van Duyne, J. Phys. Chem. Lett. **2**, 1199 (2011).
12. C. Zong, R. Premasiri, H. Lin, Y. Huang, C. Zhang, C. Yang, B. Ren, L. D. Ziegler, and J.-X. Cheng, Nat. Commun. **10**, 1 (2019).
13. P. Kumar, H. Kuramochi, S. Takeuchi, and T. Tahara, J. Phys. Chem. Lett. **11**, 6305 (2020).
14. Y. E. Monfared, T. M. Shaffer, S. S. Gambhir, and K. C. Hewitt, Sci. Rep. **9**, 12092 (2019).
15. H. Zhao, S. Clemmen, A. Raza, and R. Baets, Opt. Lett. **43**, 1403 (2018).
16. A. Dhakal, P. Wuytens, A. Raza, N. Le Thomas, and R. Baets, Materials **10**, 140 (2017).
17. K. Reynkens, S. Clemmen, A. Raza, H. Zhao, J. S.-D. Peñaranda, C. Detavernier, and R. Baets, Opt. Express **28**, 33564 (2020).
18. C. Zong and J.-X. Cheng, Nanophotonics **10**, 617 (2020).
19. M. Van Daele, M. B. E. Griffiths, A. Raza, M. M. Minjauw, E. Solano, J.-Y. Feng, R. K. Ramachandran, S. Clemmen, R. Baets, S. T. Barry, C. Detavernier, and J. Dendooven, ACS Appl. Mater. Interfaces **11**, 37229 (2019).
20. R. Wilson, B. A. Apgar, L. W. Martin, and D. G. Cahill, Opt. Express **20**, 28829 (2012).
21. D. Zhang, M. N. Slipchenko, D. E. Leaird, A. M. Weiner, and J.-X. Cheng, Opt. Express **21**, 13864 (2013).
22. H. Qian, Y. Xiao, and Z. Liu, Nat. Commun. **7**, 13153 (2016).
23. N. L. Gruenke, M. F. Cardinal, M. O. McAnally, R. R. Frontiera, G. C. Schatz, and R. P. Van Duyne, Chem. Soc. Rev. **45**, 2263 (2016).
24. A. Gaiduk, P. V. Ruijgrok, M. Yorulmaz, and M. Orrit, Chem. Sci. **1**, 343 (2010).

78.22.177.152 [to 2021-02-22 03:36:37]